

# Thermohydraulic numerical modelling of SVA interaction at the Monte Faito pyroclastic slope cover

S. Guglielmi<sup>1</sup>, M. Pirone<sup>2</sup>, A.S. Dias<sup>3</sup>, F. Cotecchia<sup>4</sup>, G. Urciuoli<sup>2</sup>

<sup>1</sup>*Direzione Generale per le Dighe e le Infrastrutture Idriche, Rome, Italy*

<sup>2</sup>*Università degli Studi di Napoli Federico II, Napoli, Italy*

<sup>3</sup>*Durham University, Durham, UK*

<sup>4</sup>*Politecnico di Bari, Bari, Italy*

**ABSTRACT:** Flow-like landslides are among the most destructive slope movements and often involve partially saturated pyroclastic soil covers overlaying carbonate bedrocks, as for many locations in Campania (Southern Italy). Prediction of the onset of these shallow landslides has often relied on semi-empirical or simplified numerical modelling, neglecting the role on landslide hazard of the hydromechanical slope behaviour, the vegetation cover, and the presence of geomorphological irregularities. This paper presents coupled thermohydraulic (TH) modelling of a pyroclastic soil cover, accounting for several slope processes that may predispose the slope to landslide activation and should be represented in physically based models of failure onset to set up reliable early warning systems. The Mount Faito test site, located in the Lattari Mountains, has been selected as a prototype slope for the geomorphological and hydromechanical scenarios of reference, given the extensive field and laboratory characterization of the soil cover available from previous studies. After validation against field monitoring data, the TH model was used to assess the annual soil water balance—a recognized preparatory factor for flow-like landslide occurrence—and to evaluate the influence of local factors on the hydro-mechanical behaviour of the slope.

**Keywords:** thermo-hydraulic modelling; pyroclastic slope; partially saturated soil

## 1 INTRODUCTION

Flow-like landslides typically occur in granular, partially saturated soils overlying bedrock, often initiating as shallow slips and evolving into flow-like movements. Rainfall infiltration is the primary trigger, reducing matric suction and shear strength until failure. Factors controlling occurrence and distribution are classified as quasi-static (predisposing) or dynamic (preparatory). Quasi-static factors, such as soil properties, bedrock seepage, and topography, define slope susceptibility and hazard distribution, while dynamic factors, including antecedent soil saturation and vegetation, govern landslide initiation (Pirone et al., 2016, 2025). Despite advances in identifying both predisposing and preparatory factors, numerical models for predicting slope failure often fail to fully capture the combined effects of these factors. The influence of vegetation is frequently misrepresented, while local features such as buried morphology and surface irregularities are typically neglected.

This paper presents a coupled thermo-hydraulic (TH) model of a pyroclastic slope at Mount Faito, in the Lattari Mountains of southern Italy. The model simulates water and vapor flow using Darcy's and Fick's laws, as well as heat transfer through Fourier's equation,

including phase-change effects, enabling an explicit representation of vapor flux to improve evaporation estimates. Vegetation is modeled by distributing transpiration along the root zone, while the real longitudinal slope profile is incorporated to account for local topographic and morphological factors.

Guglielmi et al. (2023) validated this model against one year of field monitoring data. They integrated their outputs into limit equilibrium analyses to estimate variations in safety factors under varying weather conditions. In this paper, the TH model results are further processed to assess the annual soil water balance and to evaluate the role of local factors in controlling the hydro-mechanical behaviour of the slope.

## 2 TEST-SITE AND SOIL PROPERTIES

The test site, on Mount Faito's northern slope (40°40'32.29"N, 14°28'23.35"E), represents typical western Campania conditions prone to shallow landslides (Figure 1a). It features a fractured limestone bedrock overlain by a 1–2 m pyroclastic cover from the 79 AD eruption, with slopes of 27°–35° at 826–870 m a.s.l. (Forte et al., 2019). The cover includes A1, a shallow silty sand layer; A2, silty sands rich in brown

pumice; B, coarse white pumices; and C, older volcanic material subdivided into C1 (yellowish silty sands) and C2 (reddish-brown clayey ash) (Figure 1d).

The site is vegetated with mature *Castanea sativa* and an understory of *Pteridium aquilinum*, cleared each October. Vegetation grows from mid-April to September, peaking in July, declines in autumn, and remains dormant primarily from November to April, resuming growth in spring (Dias et al., 2022) (Figure 1e, f).

Two monitoring zones, cell 1 and cell 2 (Figure 1b, c), were equipped with five instrumented vertical profiles each to measure matric suction and volumetric water content in the pyroclastic cover. In each cell, three instrumented profiles were aligned along the slope (N, C, S), and two were positioned laterally (W, E). Measurements were obtained using 42 TDR probes and 40 tensiometers (Jetfill and SDEC France) installed at similar depths. Weekly measurements were collected manually from February 2017 to March 2019. Soil temperature was monitored at depths of 0.1, 0.2, 0.5 and 1 m along the vertical profile VA (Figure 1d), while meteorological data were recorded hourly at a nearby weather station located at 850 m a.s.l. (Pirone et al., 2025). The layout of the instrumentation is shown in Figure 1d. The geotechnical properties of the soils are summarized in Table 1. All the soils are highly porous, except for layer C2, which contains a greater amount of fine particles. Laboratory tests determined saturated permeability values for layers A1, A2, and C1, ranging from  $6.0 \times 10^{-7}$  to  $2.0 \times 10^{-6}$  m/s, which is consistent with the permeability of soils from other sites in Campania. The critical-state friction angle ( $\phi'$ ) was determined for all layers, except the pumice, through direct shear tests on saturated samples (Forte et al., 2019). The measured values range between  $35^\circ$  and  $39^\circ$ .

Table 1. Geotechnical soil properties ( $G_s$ : specific gravity of soil particles;  $n$ : porosity;  $\gamma_d$  dry unit weight;  $k_{sat}$  saturated hydraulic conductivity;  $\phi'$  friction angle;  $c'$  soil cohesion)

Soil	$G_s$	$n$	$\gamma_d$ ( $\text{kN/m}^3$ )	$k_{sat}$ (m/s)	$\phi'$ ( $^\circ$ )	$c'$ (kPa)
A1	2.60	0.65	9.10	$2.0 \times 10^{-6}$	38.4	-
A2	2.68	0.72	8.19	$1.6 \times 10^{-6}$	38.4	-
B	2.55	0.80	4.80	$1.0 \times 10^{-3}$	41.0	-
C1	2.65	0.66	7.35	$6.0 \times 10^{-7}$	35.4	-
C2	2.65	0.46	14.20	$2.8 \times 10^{-8}$	35.0	5

### 3 THERMOHYDRAULIC (TH) MODEL

Guglielmi et al. (2023) established a 2D finite element model using Vadose/W (Krahn, 2004a) to simulate coupled heat and water flow in the soil (Wilson et al., 1994). Coupling was achieved through the soil vapor term, which represents the partial pressure of water vapor ( $P_v$ ). This TH model accurately describes the SVA interaction, providing accurate estimations of both evaporation and transpiration, which are considered as vapor flux. The FAO-Penman-Monteith method (Allen et al., 1998) was applied to preprocess reference evapotranspiration ( $PET_0$ ) according to plant type and growth stage, with  $PET$  calculated as  $PET_0$  multiplied by the crop coefficient ( $k_{cb}$ ). Then,  $PET$  was divided into potential transpiration (PT) and potential evaporation (PE) based on the leaf area index (LAI). PT was vertically distributed using a root distribution function and converted into actual transpiration (AT) by considering plant moisture limitations, i.e. reduction of root water uptake as suction increases. Actual evaporation (AE) was calculated by reducing PE according to soil suction, temperature, and relative humidity ( $h_a$ ) determined by the code at the soil surface:

$$\frac{AE}{PE} = \frac{P_v/P_{vs} - h_a}{1 - h_a} \quad (1)$$

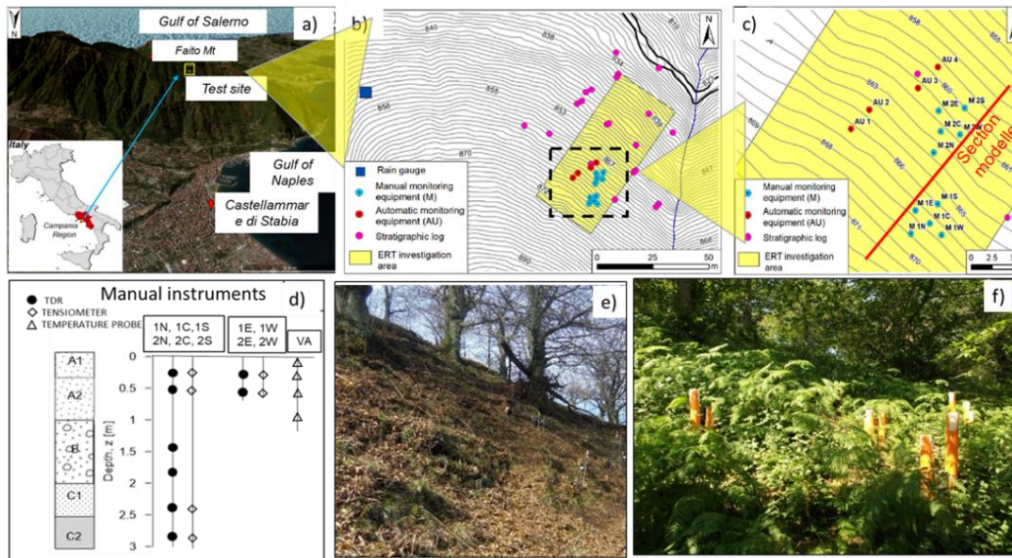


Figure 1. Test site overview: (a) location of the test site; (b) map of the area investigated with locations of the monitoring equipment, stratigraphic logs and ERT investigation area; (c) detail of the monitoring equipment distribution; (d) layout of the manual instrumentation installed; (e) vegetation at the test site on February 17, 2017; (f) on July 19, 2017

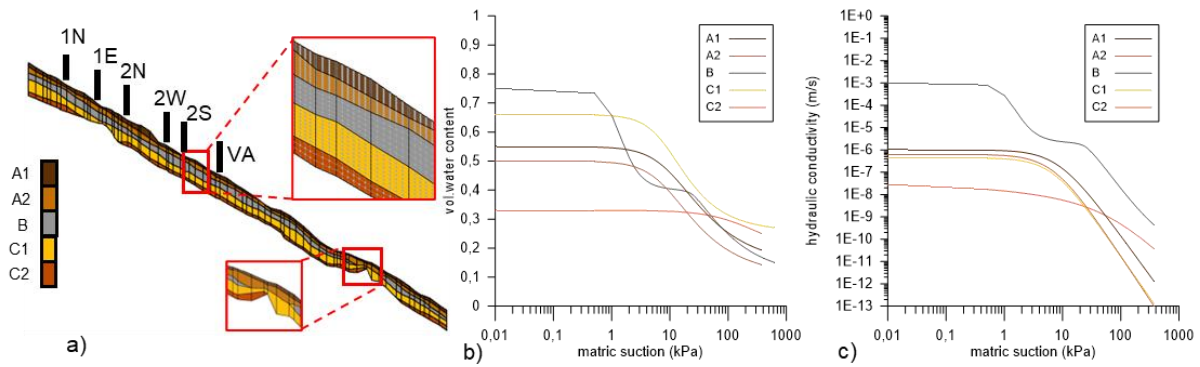


Figure 2. (a) Geometry of the analysed slope section; (b) water retention and (c) hydraulic conductivity curves

Further details on the numerical modeling are available in Guglielmi et al. (2023).

The analyzed slope section and the soil hydraulic properties adopted in the model are shown in Figure 2a–c. The water retention curve for layer B was modeled as a bimodal function. All water retention curves were defined as scanning paths by coupling field measurements of volumetric water content and suction at similar depths, as reported by Guglielmi et al. (2023). Vegetation parameters, including LAI and  $k_{cb}$  evolution, were derived from field surveys (Dias et al., 2022).

A 1 m deep root zone with a triangular water uptake profile was assumed. Initial groundwater conditions were set through a steady-state seepage analysis based on suction and temperature measurements collected in September 2017. Transient analyses were conducted from October 2017 to March 2019 using weather data collected at the site. At the base of layer C2, a matric-suction–time function was imposed as the bottom boundary condition using field data from the same layer. The effects of initial conditions became negligible after three months; therefore, results were discussed for the period January 2018–March 2019.

Guglielmi et al. (2023) validated the TH model against one year of field monitoring data. They integrated outputs into limit equilibrium analyses using Slope/W (Krahn, 2004b) to estimate variations in the safety factor under different weather conditions.

As an example, Figure 3 compares simulated daily suction, soil temperature, and volumetric water content (VWC) for layers A1 and A2 along vertical profile 2S (Figure 1c) with field measurements. The model accurately reproduces the temporal evolution of all field data, confirming its reliability for predicting soil hydraulic behaviour.

#### 4 DISCUSSION

In this paper, the TH model outputs were used to assess the 2018 soil water balance for the pyroclastic cover, which is recognized as a preparatory factor for slope failure (Figure 4). Predicted flows—precipitation (P), soil water storage ( $\Delta S$ ), actual evaporation (AE), transpiration (AT), runoff ( $R_{off}$ ), and lateral/bottom fluxes (BF)—are negative when directed outward from slope boundaries. During winter, low suctions and high volumetric water content (VWC) result in minimal  $\Delta S$ , with AE and AT near zero. Consequently, P nearly equals BF, indicating that infiltrating water mainly passes through the cover without significantly altering VWC. In spring, AE rises slightly, while AT increases sharply;  $\Delta S$  becomes negative and closely follows AT, indicating that transpiration is the dominant water loss mechanism.

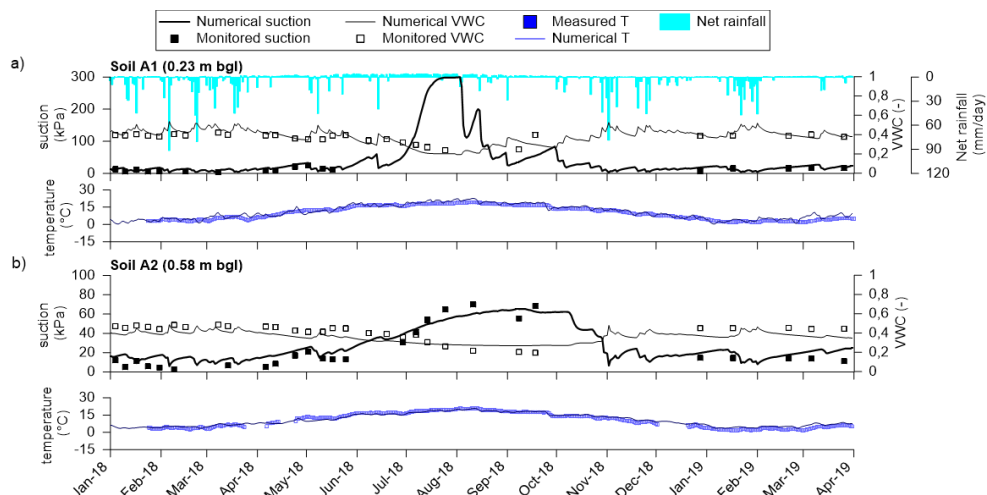


Figure 3. Monitored and calculated values of suction and VWC along vertical 2S and of mean daily temperatures along vertical VA in: (a) A1 soil; (b) A2 soil. Net rainfall is reported on the secondary y-axis in (a)

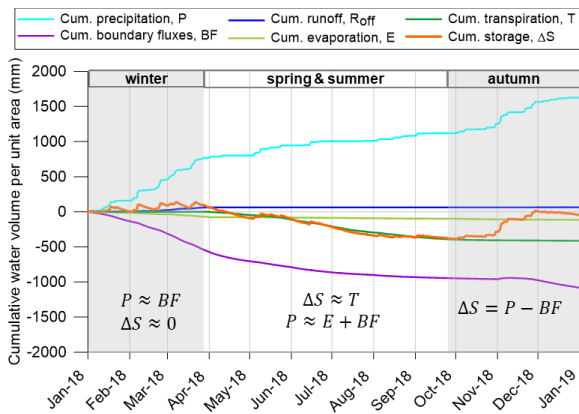


Figure 4. Soil water balance for the entire domain

In autumn,  $P$  rises again, whereas  $AE$ ,  $AT$ , and  $BF$  remain stable, and  $\Delta S$  approaches zero as rainfall replenishes the soil.  $R_{off}$  remains negligible throughout the year.

In Figure 5, maps of volumetric water content (VWC) for four different seasons of 2018 are presented. The effects of local factors are particularly evident in winter,

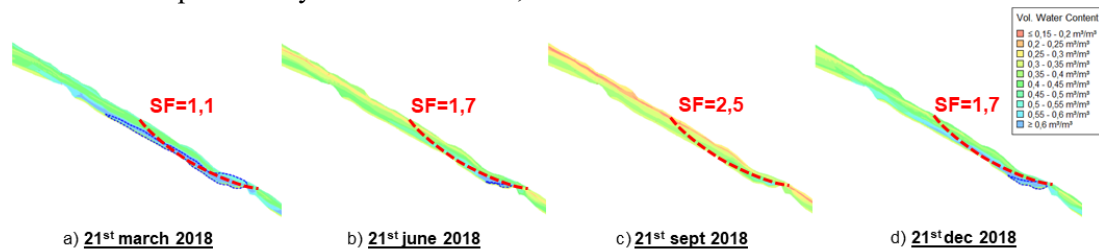


Figure 5. Maps of volumetric water content calculated on: (a) 21<sup>st</sup> March, (b) 21<sup>st</sup> June, (c) 21<sup>st</sup> September and (d) 21<sup>st</sup> December 2018. Indications of the critical slip surface and the value of SF are superimposed

## 5 CONCLUSIONS

The slope water balance on a yearly scale was determined for a pyroclastic cover susceptible to shallow slip by using TH numerical modelling. The results show that most rainfall during the wet season drains through the fractured limestone bedrock, while autumn precipitation replenishes the water lost over summer. VWC maps, along with the identification of critical slip surfaces, demonstrate the influence of local stratigraphic and morphological features on the initiation of slope failure. These findings emphasize the importance of identifying local factors that predominantly control groundwater conditions, which are crucial for accurately assessing slope stability.

## 6 REFERENCES

Allen, R.G., Pereira, L.S., Raes, D., Smith, M. 1998. Crop evapotranspiration-Guidelines for computing crop water requirements FAO Irrigation and drainage paper 56, *FAO* **300**(9), D05

Dias, A.S., Pirone, M., Nicotera, M.V., Urciuoli, G. 2022. Hydraulic characterization of an unsaturated vegetated soil: The role of plant roots and hydraulic hysteresis, *Geomech. Energy Environ.* **30**(Jun), 100235.

when a higher degree of soil saturation is observed. Figure 5a clearly illustrates how the decrease in the thickness of the pyroclastic cover influences the VWC distribution: a local groundwater lens develops upslope, causing groundwater accumulation along the slope. This area represents a critical zone for the initiation of flowslides. The lens gradually diminishes by late spring and disappears by late summer (Figure 5b,c), re-establishing in December (Figure 5d), depending on the amount of autumn rainfall.

To highlight the influence of local factors on slope stability, Guglielmi et al. (2023) used the TH model outputs in Slope/W (Krahn, 2004b) limit equilibrium analyses to estimate daily Safety Factor (SF) values for multiple circular slip surfaces from January 2018 to March 2019. For the four dates analyzed in Figure 5, the critical slip surface and corresponding SF values are superimposed on the maps. The minimum SF occurred in winter, and the critical slip surface was located in the lower slope, where the groundwater lens forms due to the reduction of cover thickness.

Forte, G., Pirone, M., Santo, A., Nicotera, M.V., Urciuoli, G. 2019. Triggering and predisposing factors for flow-like landslides in pyroclastic soils: The case study of the Lattari Mts. (southern Italy), *Eng. Geol.* **257**(Jul), 105137.

Guglielmi, S., Pirone, M., Dias, A.S., Cotecchia, F., Urciuoli, G. 2023. Thermohydraulic numerical modeling of slope-vegetation-atmosphere interaction: Case study of the pyroclastic slope cover at Monte Faito, Italy, *J. Geotech. Geoenviron. Eng.* **149**(11), 05023005.

Krahn, J. 2004a. *Vadose zone modeling with VADOSE/W: An engineering methodology*. Calgary, AB, Canada: GEO-SLOPE/W International.

Krahn, J. 2004b. *Stability modeling with SLOPE/W: An engineering methodology*. Calgary, AB, Canada: GEO-SLOPE/W International.

Pirone, M., G. Urciuoli. 2016. Cyclical suction characteristics in unsaturated slopes. *Proc., Int. workshop on Volcanic Rocks and Soils*, 183–184. London: Taylor & Francis.

Pirone, M., Forte, G., Santo, A., Urciuoli, G. 2025. Novel Rainfall Thresholds for Shallow Slip Prediction Based on Field Monitoring: Case Study of the Lattari Mountains, Italy, *Journal of Geotechnical and Geoenvironmental Engineering* **151**(3).

Wilson, G.W., Fredlund, D.G., Barbour, S.L. 1994. Coupled soil atmosphere modeling for soil evaporation, *Can. Geotech. J.* **31**(2), 151–161.